

A too-many dwarf satellite galaxies problem in the MATLAS low-to-moderate density fields

Kosuke Jamie Kanehisa^{1,2}, Marcel S. Pawlowski¹, Nick Heesters³, and Oliver Müller³

¹ Leibniz-Institut für Astrophysik Potsdam (AIP), An der Sternwarte 16, 14482 Potsdam
e-mail: kkanehisa@aip.de

² Institut für Physik und Astronomie, Universität Potsdam, Karl-Liebknecht-Straße 24/25, 14476 Potsdam, Germany

³ Institute of Physics, Laboratory of Astrophysics, Ecole Polytechnique Fédérale de Lausanne (EPFL), 1290 Sauverny, Switzerland

Accepted April 11, 2024

ABSTRACT

Context. Dwarf galaxy abundances can serve as discernment tests for models of structure formation. Previous small-scale tensions between observations and dark matter-only cosmological simulations may have been resolved with the inclusion of baryonic processes; however, these successes have been largely concentrated on the Local Group dwarfs the feedback models were initially calibrated on.

Aims. We investigate whether the Λ CDM model can reliably reproduce dwarf abundances in the MATLAS low-to-moderate density fields that are centred upon early-type host galaxies beyond the Local Volume.

Methods. We carried out mock observations of MATLAS-like fields with the high-resolution hydrodynamic simulation IllustrisTNG50. We used matching selection criteria and compared the properties of dwarfs contained within them with their MATLAS analogues.

Results. Although simulated MATLAS-like dwarfs demonstrate photometric properties that are consistent with the observed galaxy population and follow the same scaling relations, TNG50 underestimates the number of dwarf galaxies in isolated MATLAS fields at the 6σ level. This significance is maintained within crowded fields containing more than a single bright host. Our 55–62% estimate of the fraction of background galaxies is in agreement with estimates by MATLAS, but is wholly insufficient to alleviate this discrepancy in dwarf abundances. Any incompleteness in the observed fields further exacerbates this tension.

Conclusions. We identified a "too-many-satellites" problem in Λ CDM, emphasising the need for the continued testing and refining of current models of galaxy formation in environments beyond the Local Group.

Key words. Galaxies: dwarf – Galaxies: abundances

1. Introduction

The concordance Λ CDM model has been largely successful in matching astrophysical observations at cosmological scales, such as the accelerated expansion of the Universe (Planck Collaboration et al. 2016), the CMB power spectrum (Spergel et al. 2007), and filamentary large-scale structure (Tempel et al. 2014). However, comparing the expectations from cosmological simulations with observed galaxies and their dwarf satellites has revealed a number of tensions at galactic scales (Bullock & Boylan-Kolchin 2017; Sales et al. 2022).

Abundances of dwarf galaxies are particularly sensitive to the feedback prescription adopted. In the 'missing satellites' problem, dark matter-only simulations predict many more subhalos around Milky Way and M31-mass galaxies than what has been observed with respect to dwarf satellites (Klypin et al. 1999; Moore et al. 1999). This discrepancy arises from the quenching of galaxy formation in low-mass subhalos from gas heating due to the UV background from cosmic reionisation (Bovill & Ricotti 2009; Revaz & Jablonka 2018). Modern hydrodynamical and high-resolution Λ CDM simulations consistently match the luminosity function of the Milky Way and M31 dwarfs; thus, there no longer appears to be a 'missing satellites' problem within the Local Group (Engler et al. 2021).

Conversely, we are faced with a 'too-big-to-fail' (TBTf) problem (Boylan-Kolchin et al. 2011) with respect to the high-

mass end of the subhalo mass function. The dark matter masses of the brightest Milky Way satellites, as inferred from their internal velocities, are significantly lower than the most massive subhalos around simulated analogues (Boylan-Kolchin et al. 2012). These dark subhalos are sufficiently massive to enable the effective cooling of their gas content and, thus, they are too big to fail in forming visible galaxies. Yet, with baryons, the increased host galaxy potential enhances the tidal stripping and mass loss of their satellites (Brooks & Zolotov 2014), while the formation of cored profiles effectively reduce the host halo mass and, accordingly, the expected subhalo abundance (Peñarrubia et al. 2010). There is now a consensus among modern hydrodynamic simulations that there is no TBTf problem for Milky Way and M31-mass hosts (Sawala et al. 2016; Samuel et al. 2020); however, we refer to Pawlowski et al. (2015) for an alternative viewpoint.

Since the baryonic solutions implemented in cosmological simulations are calibrated for Local Group-like environments, we highlight the need to verify whether these successes remain robust beyond our cosmic neighbourhood. For instance, Smercina et al. (2018) searched for dwarfs within 150 kpc of the Milky Way-mass spiral galaxy M94 ($D = 4.2$ Mpc; Radburn-Smith et al. 2011) and found only two 'classical' satellites with $M_* > 4 \times 10^5 M_\odot$. The four other comparably massive hosts with complete 'classical' samples host an average of 6–12 such satellites, and only $< 0.2\%$ of M94 analogs in the EAGLE simulation (Schaye et al. 2015) host similarly sparse satellite sys-

tems. Similarly, a study of seven low-mass spiral galaxies in the galactic neighbourhood (Müller & Jerjen 2020) found that high-resolution dark matter simulations appear to systematically overestimate the observed satellite abundances (although this discrepancy may arise from observational biases). Conversely, the satellite luminosity function around Centaurus A – a massive elliptical galaxy at 3.8 Mpc that has been the target of multiple deep surveys – is shown to be consistent with expectations from the hydrodynamic IllustrisTNG-100 simulation to within a 90% confidence interval (Müller et al. 2019).

Recently, Müller et al. (2024) studied the abundance of dwarf galaxies around M83, a barred spiral at $D = 4.9$ Mpc (Jacobs et al. 2009), with a mass (and, thus, the expected satellite abundances) that is comparable to the Milky Way values. M83 has 13 confirmed satellites within a projected separation of 330 kpc down to a limiting magnitude of $M_V = -10$ mag. M83 analogs in the high-resolution IllustrisTNG-50 simulation, however, demonstrate sparse satellite distributions with luminosity functions inconsistent with that of the M83 system at a 3σ confidence level – thus constituting the so-called ‘too-many-satellites’ problem. The actual degree of tension is likely underestimated due to incompleteness in the observed satellite sample.

These ambiguous results suggest that models of galaxy formation in Λ CDM may still struggle to consistently predict the abundances of dwarf satellites around host galaxies beyond the Local Group. And yet, the works above only consider dwarf abundances of a few individual systems, which may conceivably be over- or under-populated as a result of some unique evolutionary history. In this paper, we study dwarf galaxy abundances within the low-to-moderate density fields in the MATLAS survey (Duc et al. 2015; Habas et al. 2020; Bílek et al. 2020; Poulain et al. 2021), across a total of 150 fields centred upon early-type host galaxies beyond the Local Volume. We then mock-observe analogous fields using identical photometric selection criteria in the state-of-the-art hydrodynamic simulation IllustrisTNG-50, which features a resolution rivalling or even exceeding zoom-in simulations which consistently predict dwarf properties to the lower end of the subhalo mass function. In this way, we tested for the first time whether dwarf abundances in MATLAS are consistent with expectations from concordance cosmology.

2. Method

2.1. ATLAS^{3D} and the MATLAS survey

The Mass Assembly of early-Type gaLaxies with their fine Structures (MATLAS) deep imaging survey targets a volume-complete sample of early-type galaxies (ETGs) acquired from the ATLAS^{3D} legacy program (Cappellari et al. 2011). ATLAS^{3D} consists of 260 elliptical and lenticular galaxies with K-band absolute magnitudes of $M_K < -21.5$, selected from a parent sample of 871 massive galaxies. The targeted ETGs are located at declinations of $|\delta - 29^\circ| < 35^\circ$ and Galactic latitudes of $b > 15^\circ$, and lie within 10 – 45 Mpc ($z < 0.01$) of the Milky Way. Together with the Next Generation Virgo cluster Survey (NGVS; Ferrarese et al. 2012), MATLAS conducted deep optical imaging of the regions around the ATLAS^{3D} ETGs. NGVS mapped fields around 58 of the ATLAS^{3D} targets between 2009 and 2013, while MATLAS has since imaged most of the remaining ETGs.

The MATLAS survey consists of a total of 150 fields around 180 ETGs and 59 late-type galaxies (LTGs) from ATLAS^{3D}’s parent catalogue, each with dimensions of $63' \times 69'$ and a resolution of 0.187 arcsec pix^{-1} . Multiband observations were performed using the MegaCam on the 3.6-metre Canada-France-

Hawaii Telescope (CFHT) between 2010 and 2015 (Duc et al. 2015). MATLAS was designed to study low surface brightness features in the outskirts of the ATLAS^{3D} ETGs to a local depth in the g-band of $\mu_g = 28.5 - 29$ mag arcsec⁻² (Duc et al. 2014); therefore, it is ideal for resolving populations of faint and low-surface brightness dwarf galaxies around their massive hosts.

2.2. MATLAS dwarf catalogue

MATLAS adopts both a fully visual and semi-automatic approach to generate its dwarf catalogue. The visual approach is used purely to calibrate the dwarf selection criteria used by the latter and the authors identified 1349 dwarfs across all 150 fields. The semi-automatic catalogue first uses SOURCE EXTRACTOR (hereafter SEXTRACTOR; Bertin & Arnouts 1996) to generate an automated list of dwarf candidates, followed up by a multi-stage visual cleaning procedure. It was found that a linear cut in average surface brightness, $\langle \mu_g \rangle$, and apparent magnitude, m_g , resulted in the cleanest separation between the visually selected dwarfs and non-dwarf detections from a representative field around NGC 4382 (Habas et al. 2020). Substructures could only be identified in more massive galaxies – hence confirming their background nature – when their area was larger than 75 pix^2 (23.5 arcsec^2) and all smaller objects were removed from the selection. The catalogue was then cleaned manually by the authors and dwarfs were classified by their visual morphology.

The final dwarf catalogue contains 2210 unique dwarf candidates and is dominated by dwarf ellipticals (dE, 73.4%), while the remaining 26.6% are classified as dwarf irregulars (dIrr). One of the 150 MATLAS fields is devoid of detectable dwarfs due to intense light contamination from a nearby star. The remaining 149 fields host between 2 and 79 dwarf candidates per field. Furthermore, 67 fields contain no bright galaxies (defined by a magnitude of $< M_K + 1$), other than the field’s target ETG, while a further 22 fields lack bright galaxies in close projection to the central ETG within a square 175 kpc region.

Dwarf galaxies are generally assumed to be satellites of the central ETGs in their respective fields. There are 325 dwarf candidates (15%) with at least one independent distance estimate, spanning a range between 5.1 and 100.6 Mpc. Furthermore, 90% of these dwarfs lie within the 10 – 45 Mpc region populated by the ATLAS^{3D} ETGs. Intrinsic properties including effective radius, R_e , Sersic index, n , and axis ratio, b/a , were derived using GALFIT (Peng et al. 2010) in Poulain et al. (2021). Since a majority of the MATLAS dwarfs lack associated distances, their properties were calculated under the assumption that each dwarf is located at the same distance as their field’s targeted host galaxy. The authors confirm the dwarf nature of the catalogued objects using a cut of $M_g > -18$, and 80% of dwarfs appear to be physically associated to their field’s central ETG with a relative radial velocity within 500 km s^{-1} . Of 56 dwarfs with additional MUSE spectroscopy, 42 (75%) demonstrate radial velocities within $1000 - 3000 \text{ km s}^{-1}$, thus consistent with the ATLAS^{3D} galaxies (Heesters et al. 2023).

2.3. Host galaxy selection in TNG50

We use data from the IllustrisTNG suite¹ of large-volume hydrodynamic cosmological simulations (Pillepich et al. 2018). All runs contained therein adopt cosmological parameters taken from Planck (Planck Collaboration et al. 2016): $\Omega_\Lambda = 0.6911$, $\Omega_m = 0.3089$, and $h = 0.6774$. We specifically used the highest-

¹ Publicly available at www.tng-project.org.

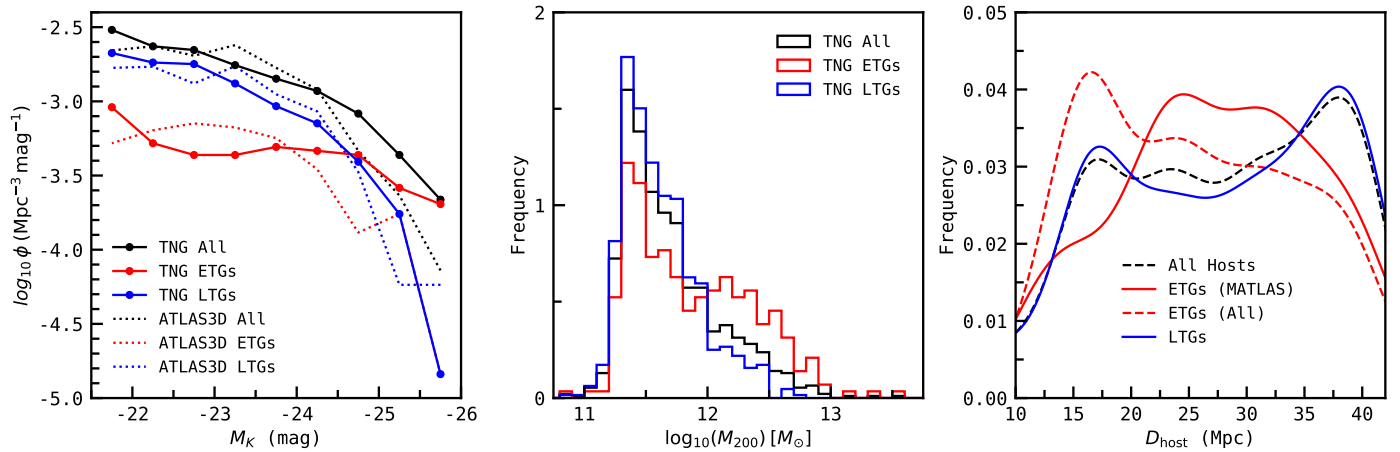


Fig. 1. Properties of ATLAS^{3D} host galaxies and their TNG50 analogues. **Left:** Luminosity functions of TNG50 and ATLAS^{3D} hosts are plotted in solid and dotted lines, respectively. The latter corresponds to Fig. 3 in Cappellari et al. (2011). Samples containing only early-type and late-type centrals are denoted in red and blue respectively. **Middle:** Mass distribution of the dark matter halos hosting the TNG50 analogues. **Right:** Distance distribution of ATLAS^{3D} targets, smoothed via a Gaussian kernel for re-sampling in this work. The MATLAS survey targets a subset of the early-type ATLAS^{3D} hosts (solid red line).

resolution TNG50 run ($L_{\text{box}} = 51.7$ Mpc) which (with a baryonic particle mass of $m_{\text{gas}} = 8.5 \times 10^4 M_{\odot}$) best resolves populations of MATLAS-like dwarfs with estimated stellar masses of $5.8 < \log_{10}(M_*/M_{\odot}) < 9$ (see Habas et al. 2020).

IllustrisTNG adopts the classic friends-of-friends (FOF) approach to identify virialised dark halos, then populating them with subhalos using SUBFIND (Springel et al. 2001). To select ATLAS^{3D}-like host galaxies in TNG50, we first identified all subhalos considered by SUBFIND to be the central subhalo of some parent halo. ATLAS^{3D}-like hosts are selected by mirroring Cappellari et al. (2011)’s criterion and adopting a K-band absolute magnitude cut of $M_K < -21.5$. Since TNG50 contains several highly luminous galaxies up to $M_K \sim -28$ that lack analogues in the parent ATLAS^{3D} catalogue, we imposed an additional constraint of $M_K > -26.0$ and recover a total of 925 TNG hosts.

We classified host galaxies by their Hubble morphology into early-types (ETGs) and late-types (LTGs). This distinction is made by referring to Zana et al. (2022)’s kinematic decomposition of $M_* > 10^9 M_{\odot}$ subhalos in TNG50 into five distinct components – the thin disc, thick disc, pseudo-bulge, bulge, and stellar halo. While the original work defines a given galaxy’s disc-to-total mass ratio D/T as the combined mass fraction of the former three rotating components, we argue that only the thin and thick disc would be observationally distinguishable; thus, we excluded the pseudo-bulge from our D/T calculation. Since there is no clear distinction between ETGs and LTGs in this metric, we took advantage of ATLAS^{3D}’s volume-complete nature and assume the fraction of observed ETGs ($260/871 = 0.299$) also holds in TNG50. The 30th percentile of the full D/T distribution at 0.575 is hence set as the threshold between early-types and late-types, and we identify 287 ATLAS^{3D}-like ETGs.

The properties of the sampled ATLAS^{3D}-like hosts in TNG50 are shown in Fig. 1. The simulated luminosity function roughly agrees with that in ATLAS^{3D} (Cappellari et al. 2011), although TNG50 demonstrates an excess of luminous early-type hosts at $M_K < -24$. The sample of TNG50 analogues appears to be dominated by Milky-Way and M31-mass objects within halos of $10^{11.5} M_{\odot} < M_{200} < 10^{12.5} M_{\odot}$.

2.4. Mock-observing MATLAS-like fields

We mock-observed $63' \times 69'$ fields centred upon the selected TNG hosts to resemble the MATLAS low-to-moderate density fields as closely as possible. ATLAS^{3D}’s distribution of the 180 ETGs targeted by MATLAS (Cappellari et al. 2011) were smoothed using a Gaussian kernel. The obtained kernel density estimate (KDE) was truncated at 10 Mpc and 45 Mpc to mirror the observed sample (see the right-hand panel in Fig. 1). We generate $N_{\text{real}} = 10$ realisations for each early-type TNG host galaxy, each with a mock-observation distance, D_{host} , independently drawn from the ATLAS^{3D} KDE.

For each realisation, we drew an observing direction, \hat{r} , from an isotropic distribution and define an associated cone with an opening angle of $\theta_{\text{field}} = 46.7$ arcmin (thus fully containing the final $63' \times 69'$ survey footprint centred upon the target host) and observation depth, D_{obs} , aligned with \hat{r} . An observer is placed at a distance of D_{host} from each ATLAS^{3D}-like host galaxy along $-\hat{r}$ and we proceeded to mock-observe all luminous subhalos within a $63' \times 69'$ field around the host across multiple periodic volumes until $D_{\text{obs}} = 100$ Mpc was reached.

Since it is unfeasible to straightforwardly replicate Habas et al. (2020)’s visual inspection of dwarf candidates for the mock-observed subhalos, we focussed on adopting the quantitative selection criteria used to compile the final MATLAS dwarf sample. The greatest challenge lies in estimating effective (half-light) radii R_e for TNG’s luminous subhalos, a rigorous approach to which would require the individual modelling of Sérsic profiles for each subhalo while accounting for their relative orientation and morphology. We instead approximated R_e with a straightforward conversion from stellar half-mass radii $R_{1/2}$, which is provided by TNG’s Subfind group catalogues. Price et al. (2022) found that the ratio between $R_{1/2}$ and R_e is generally consistent over varying Sérsic indices and, rather, it primarily depends on the galaxy’s projected axis ratio, q_0 . The full population of MATLAS dwarfs (Habas et al. 2020) demonstrates a distribution of q_0 between 0.3 and 1.0, with a median value of roughly $q_0 = 0.7$. The range of MATLAS q_0 from GALFIT covers $1.05 < R_{1/2}/R_e < 1.3$, and we adopt a corresponding static $R_{1/2}/R_e$ ratio of 1.2 (see Fig. 2 in Price et al. 2022).

The apparent g-band magnitude of TNG’s luminous subhalos is derived from their absolute magnitude M_g in the usual manner

using:

$$m_g = M_g + 5 \log_{10}(D/10\text{pc}), \quad (1)$$

when mock-observed at a distance D , although we do not account for the effects of dust attenuation. Each subhalo's average surface brightness $\langle \mu_g \rangle$ within R_e (in units of mag arcsec^{-2}) is calculated from m_g and the angular expression of R_e as:

$$\langle \mu_g \rangle = 0.75 + m_g + 2.5 \log_{10}(\pi (R_e/\text{arcsec})^2), \quad (2)$$

where the factor $2.5 \log_{10}(2) = 0.75$ arises from considering the flux observed only within R_e .

2.5. Selection criteria for MATLAS-like dwarfs

The distribution of observed MATLAS dwarfs in $\langle \mu_g \rangle - m_g$ space is plotted in the upper left panel of Fig. 2. We differentiate between dwarfs and more massive galaxies by implementing Habas et al. (2020)'s linear photometric cut of

$$\langle \mu_g \rangle \geq 0.32 m_g + 18.5. \quad (3)$$

While the authors calibrate this cut for each field to best separate the low-surface-brightness region of the main locus of galaxies with the visually confirmed MATLAS dwarfs, these shifts generally remain within $\langle \mu_g \rangle$ offsets of less than $0.1 \text{ mag arcsec}^{-2}$. Hence, we adopted Eq. 3 (blue dashed line) as a static threshold for the remainder of this work. While MATLAS is capable of detecting substructures to local depths of $\mu_g = 28.5 - 29 \text{ mag arcsec}^{-2}$, the lowest average surface brightness within R_e recorded within the final dwarf catalogue is only $26.7 \text{ mag arcsec}^{-2}$. Hence, we defined a criterion for average surface brightness of:

$$\langle \mu_g \rangle < 26.7 \text{ mag arcsec}^{-2}, \quad (4)$$

for dwarfs in the mock-observed TNG fields (green dashed line).

The region in $\langle \mu_g \rangle - m_g$ space encompassed by the two cuts defined above contains a population of visually bright galaxies at $m_g < 15$ that is not present in the MATLAS catalogue. Their absence is likely due to the visual inspection by Habas et al. (2020) correctly identifying them as non-dwarfs. Since all MATLAS dwarfs demonstrate GALFIT and SExtractor magnitudes of $m_g > 14.86$, we corrected for this discrepancy by imposing an additional, conservative cut at:

$$m_g > 15, \quad (5)$$

(red dotted line). Finally, MATLAS rejects all dwarf candidates with an ISOAREA parameter in SExtractor of 75 pix^2 . While ISOAREA has no exact physical analogue available for TNG subhalos, we find that this rejection cut corresponds to a minimum angular effective radius of:

$$R_e > 2 \text{ arcsec}, \quad (6)$$

(black dotted line) in the MATLAS catalogue, which we adopted as our last selection criteria for MATLAS-like dwarfs. This cut in R_e serves to further remove background interlopers from our sample, as only $< 0.1\%$ of physically bound MATLAS-like dwarfs are rejected in this final step.

The population of galaxies in our mock-observed TNG fields consist of satellite galaxies of the ETGs targeted by each field, as well as a fraction of interlopers – foreground or background objects that are not physically associated with their field's central galaxy. An accurate distinction can be made by whether

a MATLAS-like dwarf is considered to be bound to their presumed host galaxy's halo in SUBFIND's halo catalogue. A more observationally analogous approach uses the difference in radial velocities between the given dwarf and its field's central ETG while taking their recession velocities due to the Hubble flow into account. Habas et al. (2020) estimated that using a cut of $|\Delta v| < 500 \text{ km s}^{-1}$, around 80% of dwarf candidates with independent distance estimates appear to be satellites of the ETG or LTG with the smallest angular separation. We adopted the same threshold below to test whether we obtain a comparable fraction of physically associated dwarfs in TNG's MATLAS-like fields.

3. Results & discussion

3.1. Properties of MATLAS-like dwarfs

Mock-observed properties of TNG50 subhalos are plotted in the left-hand panels of Fig. 2. The distribution of all luminous TNG subhalos bound to their field's central host galaxy follows a roughly linear relation in $\langle \mu_g \rangle - m_g$. Dwarfs considered to be MATLAS-like lie in the region enclosed by the four selection criteria in Eqs. 3-6 and exhibit stellar masses of the order of $10^7 - 10^8 M_\odot$. The observed MATLAS dwarfs in the upper panel inhabit a region consistent with our mock-observed analogues, but extend to higher m_g for a given $\langle \mu_g \rangle$. This shift can be accounted for if a fraction of the MATLAS dwarfs are background interlopers unassociated with their supposed host galaxies. In Fig. 2, we demonstrate that these outlying MATLAS dwarfs are consistent with a background distribution at distances up to $90 - 100 \text{ Mpc}$. This maximum is in excellent agreement with the 13% of MATLAS dwarfs with independent distance estimates – which cover a range of distances up to 100.6 Mpc – and justifies our choice of observation depth of $D_{\text{obs}} = 100 \text{ Mpc}$ in Section 2.4.

The right-hand panels of Fig. 2 shows intrinsic properties of all luminous TNG subhalos. MATLAS-like dwarfs (plotted as white circles) appear to follow the standard scaling relation between M_g and R_e . The full distribution of observed MATLAS dwarfs partially lies along the region inhabited by TNG's MATLAS-like analogues, but also appreciably extends to larger M_g and lower R_e . Since 85% of MATLAS dwarfs lack distance estimates, both R_e and M_g were calculated by assuming they are located at the same distance as their supposed host galaxy (Habas et al. 2020). When making this assumption for the luminous TNG subhalos, they span a much larger region in $M_g - R_e$ space that is now consistent with the MATLAS dwarfs. The fact that the MATLAS dwarfs also extend beyond the $\langle \mu_g \rangle = 26.7 \text{ mag arcsec}^{-2}$ threshold (despite following this cut in the left-hand panels) also hints at the unreliability of their size and absolute magnitude estimates. The few MATLAS dwarfs with distance estimates (blue triangles) demonstrate a much closer alignment with TNG's MATLAS-like dwarfs and generally do not extend beyond the $\langle \mu_g \rangle$ threshold. Overall, the MATLAS-like dwarfs mock-observed in TNG50 display photometric and intrinsic properties that are fully consistent with dwarfs observed in the MATLAS fields, especially when assuming a degree of contamination by background interlopers.

3.2. MATLAS-like dwarf populations

The number of dwarf galaxies contained within the MATLAS fields depends heavily on the central host galaxy's degree of isolation. Crowded fields containing multiple ETGs and/or LTGs have enhanced dwarf counts due to the stacking of multiple dis-

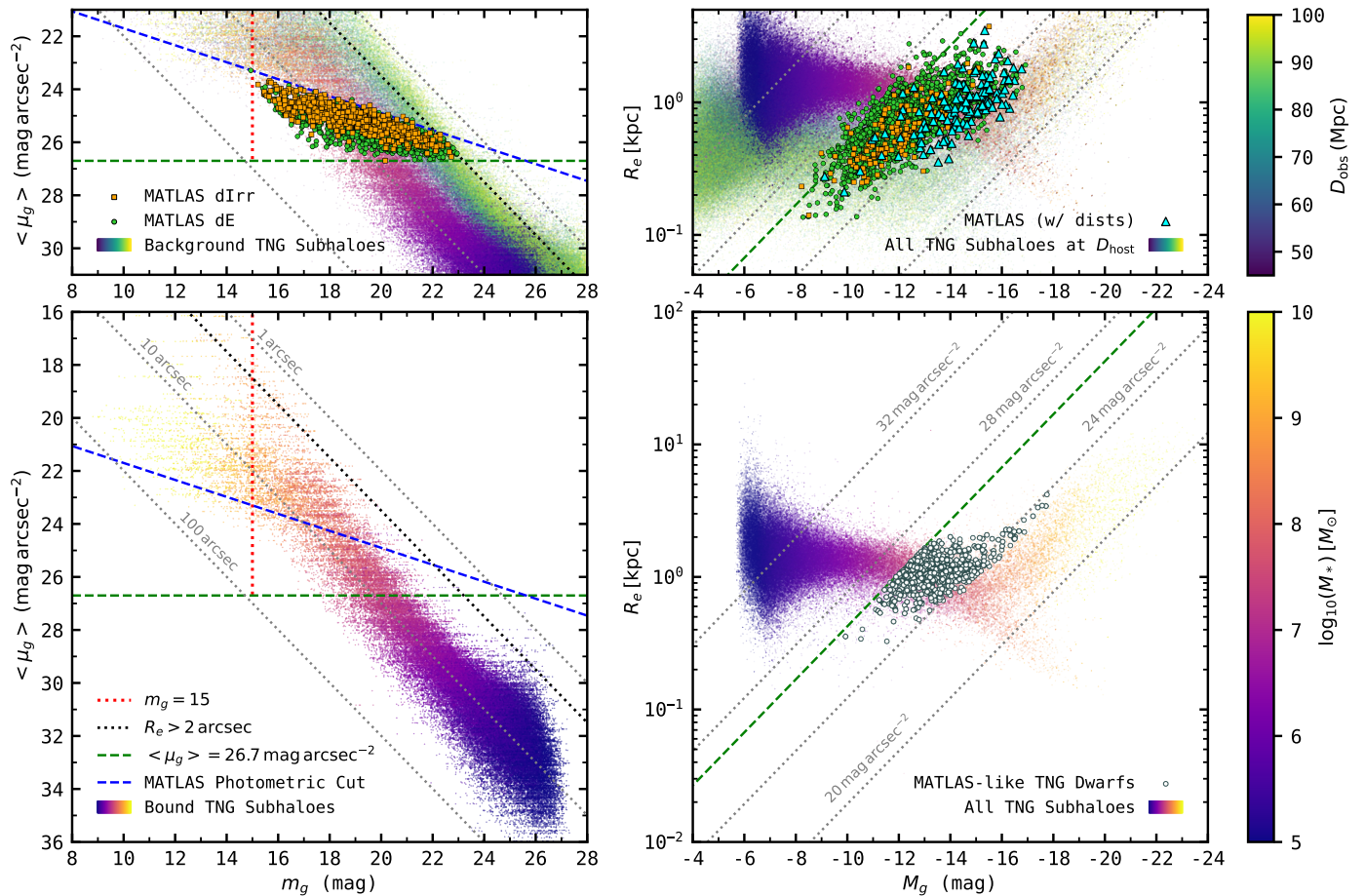


Fig. 2. Scaling relations for MATLAS dwarfs and luminous subhaloes in the TNG50 simulation. **Left:** Selection criteria for MATLAS-like dwarfs mock-observed in TNG50. The blue line indicates the linear cut between regular galaxies and dwarfs adopted in MATLAS (Habas et al. 2020). The green, red, and black lines respectively represent cuts on average surface brightness ($\langle \mu_g \rangle$), apparent magnitude m_g , and apparent effective radius motivated by the distribution of the MATLAS dwarfs (see upper panel). The observed dwarfs demonstrate photometric properties consistent with their TNG counterparts, except for a population at larger m_g than expected in the simulated $\langle \mu_g \rangle - m_g$ relation. This discrepancy can be explained by assuming that a fraction of the MATLAS dwarfs are background galaxies with distances up to 100 Mpc. **Right:** Physical properties of luminous subhalos in TNG’s mock-observed fields. MATLAS-like dwarfs that satisfy the selection criteria are indicated as white circles. Distances are not available for around 85% of the MATLAS dwarfs, and they are assumed to lie at the same distance as their field’s target host galaxy. The TNG dwarfs, when making this assumption, also follow a similar extended distribution in $R_e - M_g$ space. MATLAS dwarfs with known distances follow the true TNG distribution more closely.

tinct satellite populations. To control for this bias, we focus on fully isolated fields wherein the central ETG has no other bright galaxy with a magnitude of $< M_K + 1$ within a 3D distance of 1 Mpc – a threshold selected to distinguish isolated hosts from the Local Group pair ~ 800 kpc apart, see Appendix A. We disregarded galaxies without apparent k-band magnitudes since they are likely to lie on the fainter, low-mass end of the luminosity function. We searched for potential companion galaxies in the Heraklion Extragalactic Catalogue (HECATE; Kovelakas et al. 2021), a value-added all-sky galaxy catalogue containing over 200,000 galaxies within 200 Mpc. Thus, we identified 48 fully isolated MATLAS fields that satisfy these criteria.

The left-hand panel in Fig. 3 plots the cumulative distribution of dwarf populations in the isolated MATLAS fields (solid red line). We identified isolated MATLAS-like fields in TNG50 using the same criteria and plot their dwarf counts in black. In stark contrast to the MATLAS median of ten dwarfs per isolated field, the mock-observed TNG fields only contain a median population of three MATLAS-like dwarf galaxies. A two-sample Kolmogorov-Smirnov (KS) test reveals that the two distributions are inconsistent with being drawn from the same parent distribu-

tion at a 6.7σ confidence level ($D = 0.503$, $p = 2.9 \times 10^{-11}$). This discrepancy only widens when solely considering TNG dwarfs with radial velocities within 500 km s^{-1} of their field’s central ETG; thus, MATLAS-like fields in TNG50 are found to only contain a median of one such dwarf. When restricting our search to dwarfs bound to their field’s host galaxy, the median satellite population drops to zero. While we focus on isolated fields for this analysis, it is evident (see Fig. 3) that more crowded fields in TNG and MATLAS demonstrate a similar or greater degree of tension. We also note that this result is robust to our adopted threshold between early-type and late-type hosts, as the latter ($D/T > 0.575$) demonstrate median populations of MATLAS-like dwarfs identical to the former.

Dwarf galaxy populations in the MATLAS fields can also be described using luminosity functions (Fig. 3, central panel). Due to the large variance in the number of dwarfs per field and the discrete nature of dwarf counts, we characterised the isolated MATLAS luminosity function (red line) using the cumulative mean dwarf population brighter than a given M_g . We note that 2.8% of MATLAS dwarfs lack m_g estimates from SEXTRACTOR or GALFIT, so we indicate the true mean dwarf population per

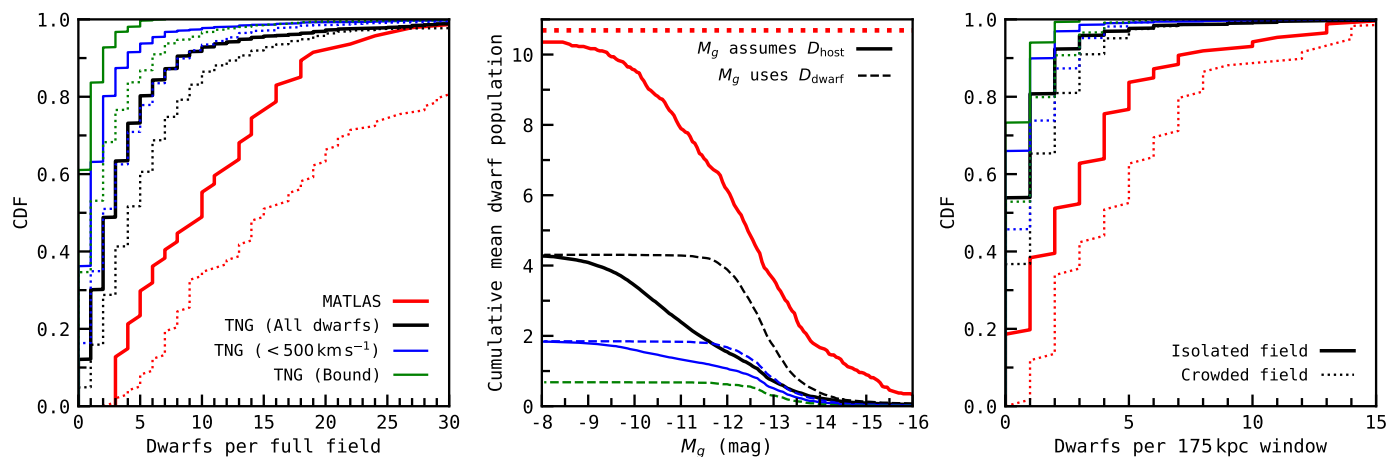


Fig. 3. Population of MATLAS-like dwarfs in TNG’s mock-observed fields is significantly lower than observed in the MATLAS low density fields. **Left:** Dwarf counts in the 63’ by 69’ MATLAS fields (red) and MATLAS-like fields mock-observed in TNG50 (black). Dwarf galaxies that appear to be physically associated with the targeted hosts (by a radial velocity difference of $< 500 \text{ km s}^{-1}$) are also shown in blue, while dwarfs bound to their host galaxy’s halo are drawn in green. Solid lines indicate fields around isolated MATLAS and MATLAS-like host galaxies that lack a companion with a magnitude of $< M_K + 1$ within 1 Mpc, while dotted lines represent the remaining fields. Dwarf populations of isolated TNG fields are inconsistent with these isolated MATLAS fields – even when including unassociated interlopers in the former – at a 7σ confidence level. **Centre:** Cumulative luminosity functions for MATLAS and TNG dwarfs in isolated fields. The solid line represents dwarf absolute magnitudes derived by assuming they lie at their supposed host galaxy’s distance (like the MATLAS dwarfs), while the dashed line adopts their true distances instead. Since around 3% of the MATLAS dwarfs lack m_g estimates, the red dotted line indicates the true mean population of MATLAS dwarfs per field. **Right:** Same as the left panel, but only counting dwarfs that lie within a square field with physical dimensions of 175 kpc centred upon each targeted host galaxy corresponding to the MATLAS field size at the near bound of 10 Mpc.

isolated field with a red dotted line. As discussed in Section 3.1, M_g is calculated for MATLAS dwarfs by assuming they lie at their presumed host galaxy’s distance, D_{host} . Solid black and blue lines correspond to TNG dwarfs under the same assumption, while dashed lines show their true M_g distribution. Solid and dashed lines are roughly equivalent for bound TNG dwarfs (green line) due to their physical proximity to their field’s central ETG and, thus, only one line is shown. To fully match TNG’s mean value of 0.74 bound satellites per isolated field, 93% of the MATLAS dwarfs would need to be interlopers unassociated with their supposed host.

The one-degree fields in MATLAS cover a region around their central host galaxy that scales linearly with observation distance – with a length ranging from 175 kpc at $D_{\text{host}} = 10 \text{ Mpc}$ to nearly 800 kpc at the maximum host distance of 45 Mpc. To compensate for this dependence, we follow Habas et al. (2020)’s method and define a square window with dimensions of 175 kpc, corresponding to the minimum physical field size around each MATLAS ETG. The distribution of dwarfs located within this 175 kpc window is plotted in the right-hand panel of Fig. 3. In contrast to the isolated MATLAS median of two dwarfs per window, over 50% of isolated MATLAS-like fields in TNG50 contain no dwarfs within their 175 kpc window. According to the 2-sample KS test, this discrepancy constitutes a 7.3σ tension between the two distributions ($D = 0.398$, $p = 3.1 \times 10^{-13}$), a significance even exceeding the tension over the full one-degree fields.

3.3. Satellite galaxies and interloper contamination

When comparing populations of dwarf galaxies in the MATLAS fields and TNG’s mock-observed analogues, the fraction of interloping background galaxies cannot be assumed to be similar a priori. The multi-stage visual inspection process in the MATLAS survey (Habas et al. 2020) can rule out a majority of highly

luminous non-dwarfs due to their distinct morphology and the presence of substructure. In TNG, however, we are limited to the use of MATLAS-like photometric cuts (Eqs. 3-6) to attempt to achieve the same result.

Habas et al. (2020) reported that 77 – 82% of MATLAS dwarfs with H1 velocities or distance estimates demonstrate radial velocities within 500 km s^{-1} of their fields’ central host galaxies. On the other hand, Heesters et al. (2023) recently obtained additional spectroscopy for 56 MATLAS dwarfs from VLT’s Multi Unit Spectroscopic Explorer (MUSE; Bacon et al. 2010), finding that a much lower estimate of 57% is likely associated with their respective fields’ central ETGs using $|\Delta_v| < 500 \text{ km s}^{-1}$. In TNG’s mock-observed fields, a similar satellite fraction of 55% of all MATLAS-like dwarfs (43% in isolated fields) satisfies the same $|\Delta_v|$ criterion, although the true fraction of dwarfs bound to their field’s central ETG is much lower at 31% (16%). This counter-intuitive result of isolated fields possessing lower association fractions is due to their targeted hosts tending towards lower halo masses (and hence smaller satellite populations); meanwhile, the number of background interlopers does not vary as strongly with the target host’s M_{200} .

We demonstrate further signs of a significant fraction of interlopers among the full sample of MATLAS dwarfs in Fig. 4, which plots the distribution of their distance-dependent properties in gray. The MATLAS dwarfs are assumed to lie at their presumed host galaxy’s distance when calculating M_g and R_e . In TNG, the bound and background sample of MATLAS-like dwarfs follow similar intrinsic distributions in both M_g and R_e . However, the background dwarfs are fully distinct from the bound satellites when assuming they lie at a distance of D_{host} . Due to the different distance ranges they inhabit, the intrinsic similarity between bound and background dwarfs also results in TNG’s two populations following distinct distributions in m_g . We note that MATLAS dwarfs with distance estimates (black dotted lines) exhibit a significant excess at higher estimated luminosities simply because brighter dwarfs are more likely to satisfy the

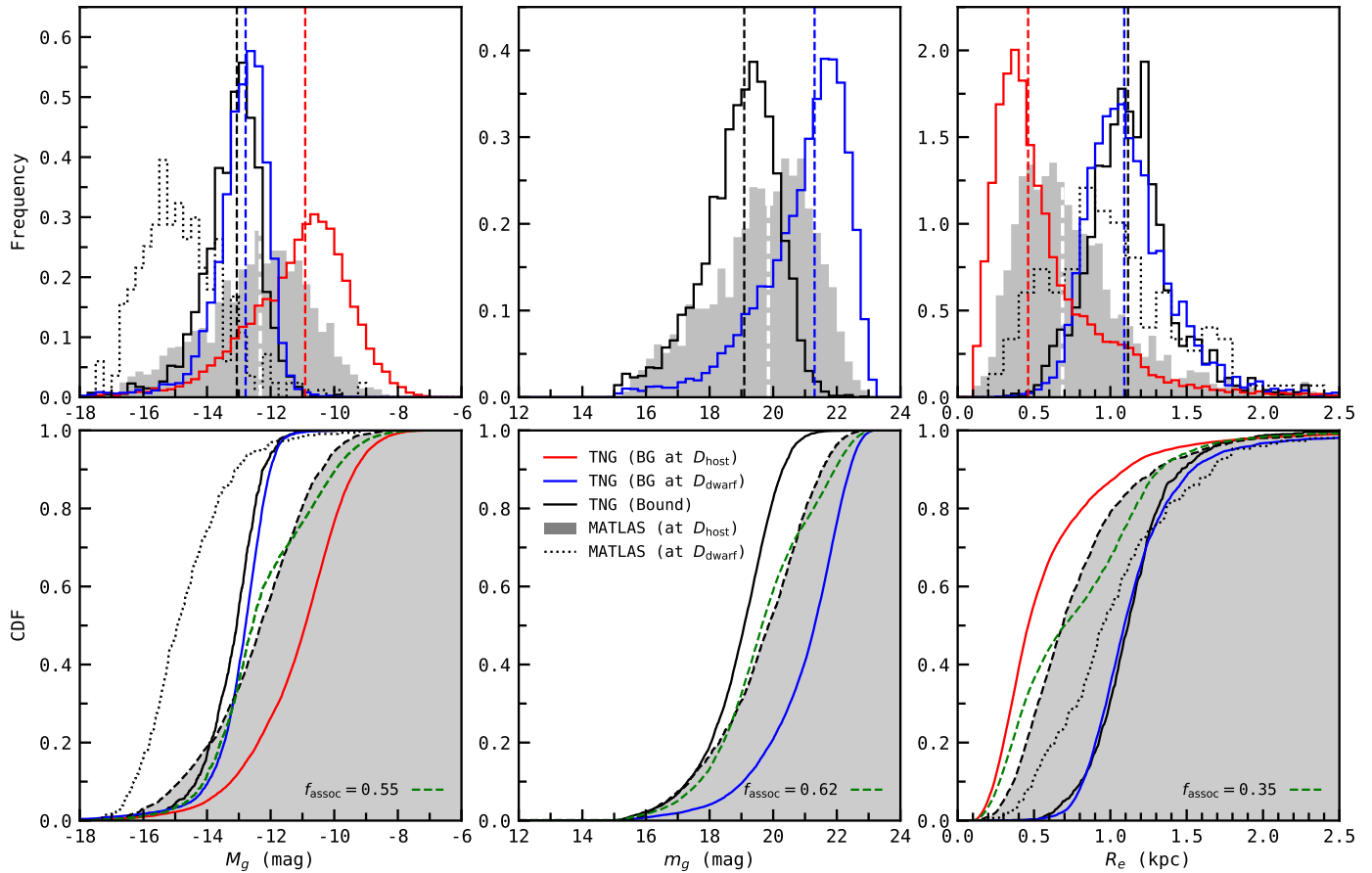


Fig. 4. Properties of the MATLAS dwarfs and their simulated TNG analogues. TNG dwarfs bound to their host galaxy are plotted in black, while those unassociated with their supposed host are drawn in blue. MATLAS dwarfs are shown in shaded grey. Absolute magnitude, M_g , and effective radius, R_e , require distance estimates to derive, while apparent magnitude, m_g , is a purely observational property. For the former two, estimates derived by assuming TNG dwarfs lie at their designated host galaxy’s distance are plotted in red. Of the MATLAS dwarfs, 15% have individual distance estimates. The M_g and R_e values calculated using these known distances are drawn as black dotted lines. The distribution of MATLAS dwarfs in M_g , m_g , and R_e generally lies between the bound and background population in TNG. We also estimate the fraction of MATLAS dwarfs physically associated to their field’s host galaxy, f_{assoc} , by averaging over TNG’s bound and background CDFs (green dashed line) with a ratio that minimizes the corresponding Kolmogorov-Smirnov statistic.

$S/N \geq 5$ requirement for their spectra (Habas et al. 2020) required to obtain sufficiently robust spectroscopic redshifts.

Since the MATLAS dwarf catalogue should consist of both bound satellites and interlopers, we may consider its distribution in each of these three properties as a superposition of TNG’s mock-observed bound and background dwarfs at some given ratio. For each property, we identify the fraction of satellites associated with their presumed host, f_{assoc} , which minimises the summed CDF’s Kolmogorov-Smirnov statistic (green dashed line) with respect to the observed MATLAS distribution (black dashed line outlining the grey region). We obtained f_{assoc} of 0.55, 0.62, and 0.35 for M_g , m_g , and R_e respectively. The optimised R_e CDF does not trace the MATLAS distribution well, and its corresponding f_{assoc} may be unreliable. Hence, we estimated that around 55–62% of all MATLAS dwarfs are associated with their field’s central ETG. This fraction is consistent with Heesters et al. (2023)’s result of 57% (although we caution that the association fraction of the brighter MATLAS dwarfs with available distance estimates may not directly translate to the full MATLAS sample). Conversely, our estimate is based on the full MATLAS dwarf sample, and remains valid if the photometric properties of the MATLAS dwarfs are consistent with their TNG analogues.

While we could attempt to alleviate the discrepancy in dwarf population between MATLAS and the mock-observed MATLAS-like fields in TNG by introducing a dominant fraction of unassociated background galaxies in the former, it seems likely that at least one-half of the observed MATLAS dwarfs are satellite galaxies of their field’s central ETG. Overall, TNG’s MATLAS-like fields demonstrate a comparable or greater degree of background contamination than MATLAS due to the lack of a visual inspection stage to remove massive interlopers with clear substructure. The tension between MATLAS and Λ CDM expectations in TNG50 remains robust at the $> 6\sigma$ level.

3.4. The impact of simulated resolution

The dearth of MATLAS-like dwarfs in TNG50 (reported in Section 3.2) may be a direct result of an insufficient simulated resolution, as well as unreliable M_g and R_e estimates derived from too few stellar particles. In Fig. 5, we demonstrate that the baryonic resolution in TNG50 is sufficient to resolve a majority of MATLAS-like dwarfs and yield realistic intrinsic properties. Habas et al. (2020) estimates the distribution of stellar masses for 658 (30%) of MATLAS dwarfs with $(g-i)$ colour estimates and clean photometry using Taylor et al. (2011)’s colour-mass rela-

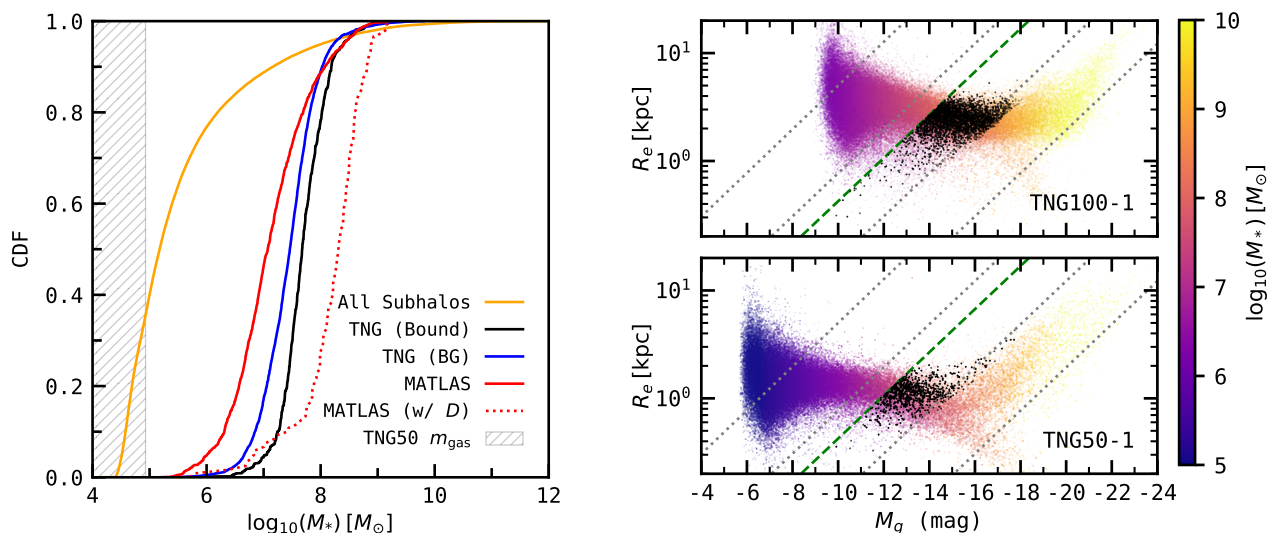


Fig. 5. **Left:** Stellar masses of TNG subhalos by their association to their supposed host galaxy (black and blue lines) and estimates for the MATLAS dwarfs from (red line; Habas et al. 2020). The latter estimates were made by assuming that the observed dwarfs lie at the same distance as their field’s target host galaxy. Stellar masses for the subset of MATLAS dwarfs for which independent distance estimates are available are plotted as a red dotted line. TNG50’s baryonic resolution m_{gas} is indicated by the hatched region. 97% of MATLAS-like dwarfs in TNG50 are sufficiently resolved with at least 100 stellar particles. **Right:** Impact of simulation resolution on dwarf populations. The lower panel is taken from Fig. 2 and shows the distribution of luminous subhalo properties in $R_e - M_g$ space in TNG50 ($m_{\text{gas}} = 8.5 \times 10^4 M_{\odot}$), while the upper panel instead displays results for the lower-resolution TNG100 run ($m_{\text{gas}} = 1.4 \times 10^6 M_{\odot}$). MATLAS-like dwarfs satisfying the selection criteria are plotted in black. The broadening in R_e due to insufficient stellar particles occurs at around $M_g > -12$ in TNG100, but only affects $M_g > -9$ in TNG50 at a regime much fainter than the MATLAS-like dwarfs.

tion (left panel, red line). The dotted red line shows the M_* estimates re-computed for MATLAS dwarfs with independent distance estimates. The former consists of a fraction of background galaxies that would systematically skew the distribution towards lower M_* , and distances are only known for the most massive, easily observed dwarfs – thus skewing the latter distribution towards higher M_* . As expected, we find the stellar masses of TNG’s mock-observed dwarfs between the two MATLAS CDFs. Finally, 97% of TNG50’s bound MATLAS-like dwarfs have a stellar mass above the equivalent of 100 stellar particles.

In the right-hand panel, we show the intrinsic scaling relation of all luminous subhalos in TNG50, as well as the lower-resolution TNG100 run ($m_{\text{gas}} = 1.4 \times 10^6 M_{\odot}$, $m_{\text{DM}} = 7.5 \times 10^6 M_{\odot}$). Dwarfs considered to be MATLAS-like in each run are plotted as black points. In both runs, we identify a broadening in the R_e distribution at higher M_g (and lower M_*) due to the difficulty in estimating the half-mass radius of a subhalo containing just a few star particles. In TNG100, this broadening begins at $M_g \sim -12$ at stellar masses within an order of magnitude of most MATLAS-like dwarfs. This is not the case for TNG50, wherein R_e appears stable beyond $M_g < -10$. We also recover a slight vertical shift in R_e over the full subhalo distribution between runs, but this is likely an artefact of the larger force softening length adopted in TNG100 (185 pc) compared to TNG50 (74 pc). Hence, we argue that TNG50 has a baryonic resolution sufficient to resolve MATLAS dwarf analogues, and the discrepancy in its simulated population with the MATLAS fields is not a direct result of unreliable M_g and $\langle \mu_g \rangle$ estimates.

4. Summary & conclusion

The MATLAS low-to-moderate density fields survey low-surface brightness dwarf galaxies around massive early-type hosts (ETGs) at distances past 10 Mpc. Thus, they serve as an

excellent testbed for satellite galaxy abundances beyond our cosmic neighbourhood. To check whether dwarf populations in MATLAS are consistent with expectations from Λ CDM cosmology, we mock-observed MATLAS-like fields in the high-resolution hydrodynamic simulation IllustrisTNG-50 using photometric selections faithful to the original survey. The simulated populations of MATLAS-like dwarfs sampled in this manner follow the standard scaling relations and demonstrate photometric properties within a range consistent with the MATLAS dwarfs, especially when assuming a 30 – 50% fraction of background interlopers unassociated with the targeted hosts.

Strikingly, the simulated fields demonstrate significantly lower abundances of MATLAS-like dwarfs than found in the survey itself. Within isolated fields which only contain a single target ETG, MATLAS has a median of ten dwarfs with surface brightnesses of $\langle \mu_g \rangle < 26.7$ mag arcsec $^{-2}$, while TNG50 only has three such dwarfs. This result constitutes the basis for the “too-many-satellites” problem in observations at the $> 6\sigma$ confidence level. We also account for the effect of host distance on the physical dimensions of the one-degree fields observed. We report that dwarf abundances within a central 175 kpc region around targeted ETGs demonstrate an similar tension at the 7σ confidence level. Furthermore, when using an viewing depth of 100 Mpc, over 50% of mock-observed TNG50 dwarfs are background interlopers that are not associated with their presumed host galaxy. On average, to match the simulated abundances of MATLAS-like dwarfs, 93% of the observed MATLAS dwarfs would need to be interlopers. This fraction is fully inconsistent with multiple estimates of the fraction of MATLAS dwarfs associated with their targeted ETG from the literature and this work, which do not drop below 50%.

In this work, we consider whether this discrepancy in dwarf populations could have arisen from systematic biases. We find that the tension is unlikely to be a straightforward artefact of simulation resolution, since TNG50 sufficiently resolves 97% of

MATLAS-like dwarfs bound to their field’s targeted host with at least 100 stellar particles. The simulated dwarfs also follow the same scaling relations as found in MATLAS (Habas et al. 2020), ruling out any significant systematic shift in their estimated effective radii. The effects of extinction from dust has not been considered, but this would further reduce the abundance of MATLAS-like dwarfs recovered in TNG50. We also do not account for the obfuscation of satellites in close projection to the central ETG, but this would similarly work to reduce TNG50’s dwarf population and compound the problem. Finally, any incompleteness in the MATLAS fields would only exacerbate the discrepancy by raising the true number of dwarfs, and the reported tension should be considered to be only a lower bound.

Our findings lie in stark contrast with Carlsten et al. (2021), who reported the satellite luminosity functions of 12 Local Volume hosts to be fully consistent with expectations from dark matter-only cosmological simulations using a stellar-to-halo mass relation from Garrison-Kimmel et al. (2017) – despite covering a similar range in host mass and satellite surface brightness. We point out, however, that we did not assess the full luminosity function of satellites around the ATLAS^{3D} ETGs, but instead we imposed strict photometric selection cuts to match our mock-observed fields with the MATLAS observations. This resulted in a comparison between better defined sub-populations of dwarf galaxies. Furthermore, Carlsten et al. (2021) adopted the lower-resolution TNG100 run as their fiducial hydrodynamic simulation, which struggles to resolve dwarfs with luminosities corresponding to the fainter MATLAS dwarfs. It is also interesting to note that the range of stellar masses in which Müller et al. (2024) reported the luminosity function of M83 to be most discrepant with theoretical predictions ($10^7 - 10^8 M_{\odot}$) coincides with the majority of MATLAS-like TNG50 dwarfs in this work. Our results suggest that models of galaxy formation within the Λ CDM framework may still struggle to reliably reproduce dwarf abundances beyond the Local Volume. Thus, the too-many-satellites problem is extended from M83 to across 150 fields in the MATLAS catalogue.

Acknowledgements. We thank A. Pillepich for interesting discussions and helpful inputs. K.J.K. and M.S.P. acknowledge funding via a Leibniz-Junior Research Group (project number J94/2020). M.S.P. also thanks the German Scholars Organization and Klaus Tschira Stiftung for support via a KT Boost Fund. O.M. and N.H. are grateful to the Swiss National Science Foundation for financial support under the grant number PZ00P2_202104. We thank the anonymous referee for their constructive input which has helped us improve the manuscript.

References

Bacon, R., Accardo, M., Adjali, L., et al. 2010, in Society of Photo-Optical Instrumentation Engineers (SPIE) Conference Series, Vol. 7735, Ground-based and Airborne Instrumentation for Astronomy III, ed. I. S. McLean, S. K. Ramsay, & H. Takami, 773508
 Bertin, E. & Arnouts, S. 1996, A&AS, 117, 393
 Bílek, M., Duc, P.-A., Cuillandre, J.-C., et al. 2020, Monthly Notices of the Royal Astronomical Society, 498, 2138
 Bovill, M. S. & Ricotti, M. 2009, ApJ, 693, 1859
 Boylan-Kolchin, M., Bullock, J. S., & Kaplinghat, M. 2011, MNRAS, 415, L40
 Boylan-Kolchin, M., Bullock, J. S., & Kaplinghat, M. 2012, MNRAS, 422, 1203
 Brooks, A. M. & Zolotov, A. 2014, ApJ, 786, 87
 Bullock, J. S. & Boylan-Kolchin, M. 2017, ARA&A, 55, 343
 Cappellari, M., Emsellem, E., Krajnović, D., et al. 2011, MNRAS, 413, 813
 Carlsten, S. G., Greene, J. E., Peter, A. H. G., Beaton, R. L., & Greco, J. P. 2021, ApJ, 908, 109
 Duc, P.-A., Cuillandre, J.-C., Karabal, E., et al. 2015, MNRAS, 446, 120
 Duc, P.-A., Paudel, S., McDermid, R. M., et al. 2014, MNRAS, 440, 1458
 Engler, C., Pillepich, A., Pasquali, A., et al. 2021, MNRAS, 507, 4211
 Ferrarese, L., Côté, P., Cuillandre, J.-C., et al. 2012, ApJS, 200, 4
 Garrison-Kimmel, S., Bullock, J. S., Boylan-Kolchin, M., & Bardwell, E. 2017, MNRAS, 464, 3108

Habas, R., Marleau, F. R., Duc, P.-A., et al. 2020, MNRAS, 491, 1901
 Heesters, N., Müller, O., Marleau, F. R., et al. 2023, arXiv e-prints, arXiv:2305.04593
 Jacobs, B. A., Rizzi, L., Tully, R. B., et al. 2009, AJ, 138, 332
 Klypin, A., Kravtsov, A. V., Valenzuela, O., & Prada, F. 1999, ApJ, 522, 82
 Kovlakas, K., Zezas, A., Andrews, J. J., et al. 2021, MNRAS, 506, 1896
 Moore, B., Ghigna, S., Governato, F., et al. 1999, ApJ, 524, L19
 Müller, O. & Jerjen, H. 2020, A&A, 644, A91
 Müller, O., Rejkuba, M., Pawłowski, M. S., et al. 2019, A&A, 629, A18
 Müller, O., Pawłowski, M. S., Revaz, Y., et al. 2024 [arXiv:2403.08717]
 Pawłowski, M. S., Famaey, B., Merritt, D., & Kroupa, P. 2015, ApJ, 815, 19
 Peñarrubia, J., Benson, A. J., Walker, M. G., et al. 2010, MNRAS, 406, 1290
 Peng, C. Y., Ho, L. C., Impey, C. D., & Rix, H.-W. 2010, AJ, 139, 2097
 Pillepich, A., Springel, V., Nelson, D., et al. 2018, MNRAS, 473, 4077
 Planck Collaboration, Ade, P. A. R., Aghanim, N., et al. 2016, A&A, 594, A13
 Poulain, M., Marleau, F. R., Habas, R., et al. 2021, MNRAS, 506, 5494
 Price, S. H., Übler, H., Förster Schreiber, N. M., et al. 2022, A&A, 665, A159
 Rادburn-Smith, D. J., de Jong, R. S., Seth, A. C., et al. 2011, ApJS, 195, 18
 Revaz, Y. & Jablonka, P. 2018, A&A, 616, A96
 Sales, L. V., Wetzel, A., & Fattahi, A. 2022, Nature Astronomy, 6, 897
 Samuel, J., Wetzel, A., Tollerud, E., et al. 2020, MNRAS, 491, 1471
 Sawala, T., Frenk, C. S., Fattahi, A., et al. 2016, MNRAS, 457, 1931
 Schaye, J., Crain, R. A., Bower, R. G., et al. 2015, MNRAS, 446, 521
 Smercina, A., Bell, E. F., Price, P. A., et al. 2018, ApJ, 863, 152
 Spergel, D. N., Bean, R., Doré, O., et al. 2007, ApJS, 170, 377
 Springel, V., White, S. D. M., Tormen, G., & Kauffmann, G. 2001, MNRAS, 328, 726
 Taylor, E. N., Hopkins, A. M., Baldry, I. K., et al. 2011, MNRAS, 418, 1587
 Tempel, E., Stoica, R. S., Martínez, V. J., et al. 2014, MNRAS, 438, 3465
 Zana, T., Lupi, A., Bonetti, M., et al. 2022, MNRAS, 515, 1524

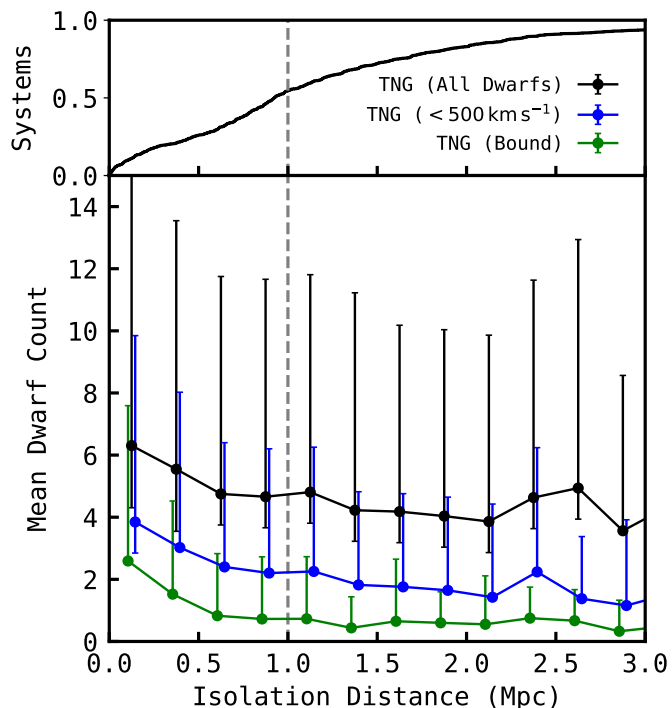


Fig. A.1. Mean dwarf populations of isolated MATLAS-like TNG50 fields, binned by the 3D distance between target hosts and their closest bright companion with a magnitude of $M_K + 1$. Black, blue, and green points correspond to samples of all MATLAS-like dwarfs, those with a radial velocity within 500 km s^{-1} of their presumed host, and dwarfs considered to be gravitationally bound to their host’s halo in `Subfind` – error bars in their respective colours denote their 1σ spread. The upper panel shows the cumulative distribution of mock-observed MATLAS-like field realisations. This work’s adopted isolation criterion of 1 Mpc is indicated by the grey dashed line.

Appendix A: Impact of host isolation

We verified whether the results obtained in this work is sensitive to our adopted isolation criterion of 1 Mpc imposed on the host galaxies mock-observed in TNG50. In Fig. A.1, we plot the mean dwarf counts in MATLAS-like fields as a function of their hosts’ distance to their closest companion. Until around 600 kpc, where the satellites of the companion host begin to encroach on the target’s dwarf population, the number of MATLAS-like dwarfs within the mock-observed fields (especially those physically associated to their presumed host galaxy) remains relatively stable. We conclude that our specific choice of 1 Mpc in our isolation criterion is unlikely to significantly contribute to the observed discrepancy in dwarf populations. Imposing a stricter degree of isolation would only serve to artificially reduce the significance of the discrepancy due to the smaller sample of MATLAS fields.